Available online at http://ajol.info/index.php/ijbcs

Int. J. Biol. Chem. Sci. 5(4): 1754-1767, August 2011

ISSN 1991-8631

International Journal of Biological and Chemical Sciences

Original Paper

http://indexmedicus.afro.who.int

Geochemistry and geochronology of the Méiganga metadiorite: implications on the timing of D2 deformational phase in Adamawa Yadé Domain in Cameroon

A. A. GANWA [1*], W. SIEBEL [2], W. FRISCH [2], C. K. SHANG [2] and G. E. EKODECK [3]

[1] *Department of Earth Sciences, University of Ngaoundéré, P.O. Box 454 Ngaoundéré, Cameroon.*
[2] *Department of Earth Sciences, University of Tübingen, Sigwartstr, 10, D72076 Tübingen, Germany.*
[3] *Department of Earth Sciences, University of Yaoundé I, P.O. Box 872 Yaoundé, Cameroon.*
[*] *Corresponding author, E-mail: ganwa1@yahoo.fr; Tel: 237 77 41 32 14*

ABSTRACT

The metadiorite of Méiganga forms an ovoid body intruding metasedimentary gneisses in the area of Méiganga city. It shows schistosity, banded structure and is made up of green hornblende, biotite, antiperthitic plagioclase, quartz, zircon, opaque minerals and chlorite. Imprints of D2, D3 and D4 deformation phases are identical in the metadiorite and the amphibole biotite gneiss, leaving no doubt as to the syn-D2 emplacement and crystallization of the protolith of the metadiorite. The metadiorite samples display high-K calc-alkaline to shoshonitic characteristics and possess features of I-type granitoids. They exhibit relative low enrichment of LREE with respect to HREE, $(La/Yb)_N$ = 9.5-11.3, and moderate negative Eu anomalies (Eu/Eu* =0.80-0.83). Optical features of the zircon grains of the metadiorite and its syn-D2 emplacement and crystallisation indicate that the zircon evaporation $^{207}Pb/^{206}Pb$ ages (614.1 ± 3.9 Ma and 619.8 ± 9.8 Ma) of this rock date the D2 deformation phase in the Méiganga area. Comparison with other sectors of the Adamawa Yadé Domain (AYD) shows the close synchronic character of the D2 deformational phase in central Cameroon (Méiganga, Tibati, Ngaoundéré areas) and the diachronic character of this phase in central and western Cameroon. We found that a similar chronological evolution has been demonstrated in the Macururé Domain of the Sergipano Belt (NE Brazil).

Keywords: syn-D2 granitoid; $^{207}Pb/^{206}Pb$ age; Central Pan-Africa Fold Belt; Sergipano Belt.

INTRODUCTION

The main structural feature of the Central Africa Fold Belt (CAFB) is the presence of regional transcurrent shear zones. These unconformities have been used to fix the boundaries between different domains of the belt: the Tcholliré-Banyo shear zone (TBSZ) is considered as border between the west Cameroon domain (WCD) and the Adamawa-Yadé domain (AYD), whilst the Sanaga shear zone (SSZ) separates the AYD from the Yaoundé domain (YD) (Toteu et al., 2004) (Figure 1). In Cameroon, those unconformities have also been used to differentiate the Panafrican basement into a northern, central and southern domain (Nzenti, 1994).

The AYD is characterised by the widespread occurrence of granitoids, which have been classified according to deformation

DOI : http://dx.doi.org/10.4314/ijbcs.v5i4.37

state into syn-tectonic, late tectonic and post-tectonic intrusives (Lassere, 1961; Toteu et al., 2001). Syn-tectonic metadiorites are widely distributed in the cameroonian portion of the AYD. The basement of the AYD consists of Paleoproterozoic metasedimentary rocks and orthogneisses which are preserved as remnants in the Mbé and Méiganga areas (Penaye et al., 1989; Ganwa, 2005). Detailed petrographic and geochronologic studies exist for a few plutons in the southwestern part of the AYD (Nguiessi Tchankam et al., 1997; Tagne-Kamga et al., 1999; Tagne-Kamga, 2003; Nzolang et al., 2003; Djouka Fonkwé et al., 2007). In the Tibati area in central Cameroon, and in western Cameroon, few syn-kinematic plutons crop out in close vicinity to the Panafrican Adamawa ductile shear zone (Central Cameroon Shear Zone: CCSZ; Nzenti et al., 2006; Njanko et al., 2006, 2010; Kwekam et al., 2010). They are high-K calc-alkaline plutons and show geochemical similarities to other Panafrican high-K calc-alkaline syn-kinematic plutons from western Cameroon. Three main successive tectonic events associated with the Panafrican collisional and post-collisional evolution are identified in Cameroon: (i) crustal thickening (ca. 630-620 Ma); (ii) left lateral wrench movement (ca. 613-585 Ma), and (iii) right lateral wrench movement (ca. 585-540 Ma) (Ngako et al., 2008).

This paper presents the results of geochemistry and a single zircon Pb evaporation study of a metadiorite from the Méiganga area. The aim was to constrain the age of the D2 deformation in the study area and, on a larger scale, to characterize its evolution in the AYD, given that the D2 is the most important deformational phase in the Panafrican metamorphic history in Central Africa.

MATERIALS AND METHODS

Analytical methods

Major and trace elements were analysed by X-ray fluorescence (XRF) at the University of Tübingen, Germany. Rare-earth elements were analysed by Inductively Coupled Plasma–Atomic Emission Spectrometry (ICP–AES) at the CRPG (Centre de recherches pétrographiques et géochimiques, Vandoeuvre-lès-Nancy, France). Analytical precisions are typically better than 2% for major elements except for P and Mn which have precisions better than 15%, and 5–10% for most trace elements. Zircon grains were separated from the 63-200 µm sieved rock fractions by standard separation techniques (milling, wet shaking table, magnetic and heavy liquid separation) and finally handpicking under the binocular microscope. Cathodoluminescence images were performed on an electronic microscope LEO Model 1450 VP (variable pressure) 4-Quadrant BSE-Detector working with an accelerating voltage of 10 kV. For zircon Pb evaporation, single zircon grains were analysed using a double Re filament configuration. Principles of the evaporation method were described by Kober (1986, 1987). Measurements were done using a Finnigan MAT 262 mass spectrometer equipped with a MassCom ion counter at the University of Tübingen. All $^{207}Pb/^{206}Pb$ ratios were corrected for common Pb according to Cocherie et al. (1992), and the error for a single zircon age was calculated after Siebel et al. (2005). Repeated measurements on natural zircon from Phalaborwa, South Africa (Kröner and Willner, 1998), and from zircon standard 91500 of 'Kuehl Lake' (Canada) (Wiedenbeck et al., 1995) were performed for geologically realistic age and error treatment (Chen et al., 2002). The results were similar to those obtained by previous authors (Kröner and Willner, 1998; Wiedenbeck et al., 1995).

Petrography and structural characteristics of the metadiorite

The metadiorite constitutes the basement of Méiganga town and its neighbourhood (Figure 2). It forms an ovoid body stretching in NE-SW direction. The magmatic body intrudes amphibole biotite gneisses (ABGn) and spatially associated to pyroxene-amphibole-biotite granites (PABGr) and biotite-muscovite granites (BMGr). With

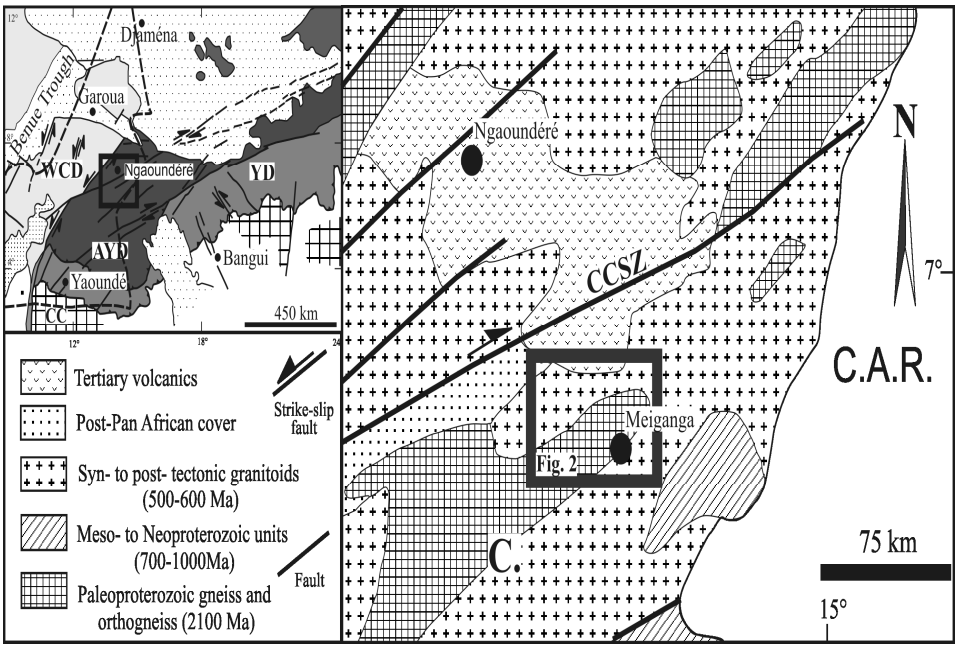

Figure 1: Geological sketch map of East Adamawa showing the Méiganga area.
Patterns are as follows: grids, Congo craton (CC); dark grey; Adamawa–Yadé Domain (AYD); medium grey, Yaoundé Domain (YD); light grey, West Cameroon Domain (WCD); Central Cameroon Shear Zone (CCSZ); heavy dots, Cameroon Line; light dots, Mesozoic sediments. The square in the inset localizes the large figure. Cameroon (C.), Central African Republic (C.A.R.)

respect to the state of deformation, the granites are posterior to the metadiorite. Studies on the various host rocks have been performed by Ganwa (2005).

The metadiorite is medium grained and shows a schistosity and a banded structure defined by quartzofeldspathic layers as a result of migmatization. Plagioclase is antiperthitic and contains submicroscopic inclusions. Quartz is partly recrystallised and forms polycrystalline ribbons parallel to the schistosity. Chlorite and opaque minerals are formed at the expense of biotite.

The metadiorite has been affected by three deformation phases (D2, D3, D4), contrary to the host gneisses which were also affected by D1. The metadiorite shows a penetrative S2 foliation marked by alternation of ferromagnesian minerals (biotite, amphibole) and quartzofeldspathic minerals. S2 in the metadiorite is parallel to S2 in the host gneisses with few exceptions. It dips between 30° and 90° towards NW to N or S to SE (Figure 2). The L2 lineation is characterized by stretching of quartz, elongate aggregates of quartz and feldspar, and the alignment of amphibole and biotite. L2 has a weak to moderate angle of plunge (up to 40°) towards NE or SW. Moreover, it shows the same orientation as in the host gneisses (Figure 2).

In the metadiorite and the host gneisses, D3 is represented by folds (F3) and an axial plane foliation (S3). The folds also affected the granite dykes. It is likely that previous schistosity planes were transposed by S3 and behave as composite S2/S3 surface.

The last deformation phase D4 was brittle. This phase produced joints and faults present at outcrop scale in all rock types. The faults are normal dextral strike-slip faults. They indicate a NE-SW distensional movement.

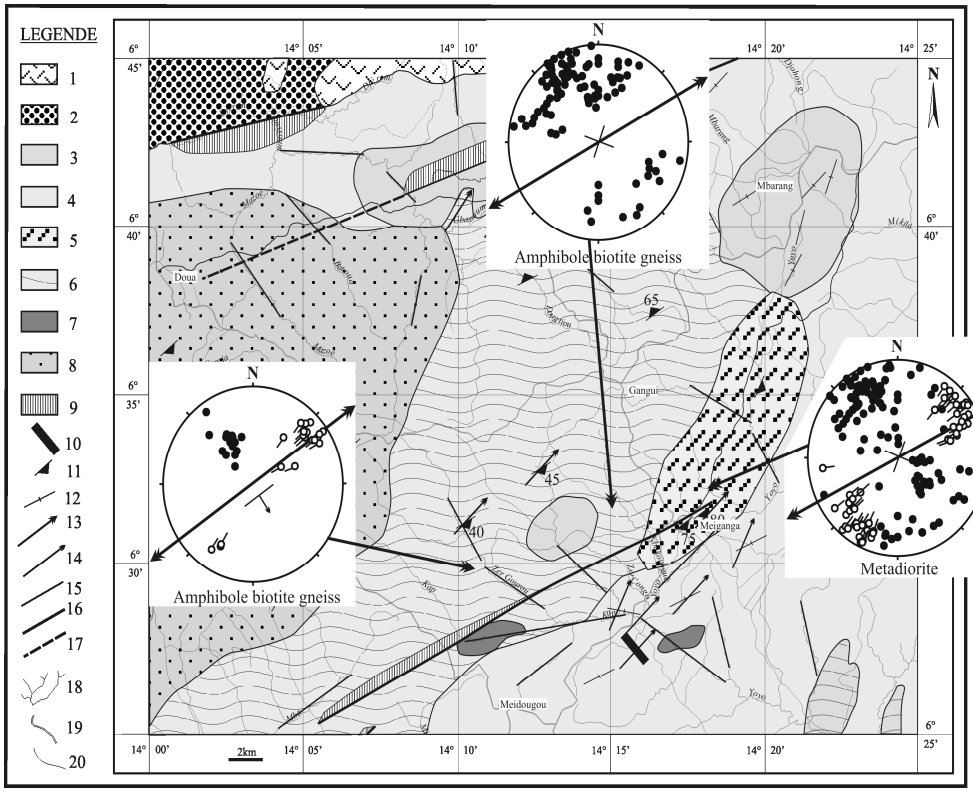

Figure 2: Geological map of Méiganga area showing stereonet of structural data in metadiorite and amphibole biotite gneiss.

(1) basalt, (2) conglomerate, (3) biotite–muscovite granite, (4) pyroxene–amphibole–biotite granite, (5) Metadiorite, (6) amphibole–biotite gneiss, (7) amphibolite, (8) pyroxene–amphibole gneiss, (9) mylonite, (10) dolerite, (11, 12) schistosity, (13, 14) lineations, (15) fractures, (16) fault, (17) supposed fault, (18) rivers, (19) road, (20) path. In the stereonet: filled circle = S2 pole, open circle with line: L2 lineation. Double arrow represents the strike of axial plane of the regional F3 fold.

The lack of the D1 imprint in the metadiorite indicates that its emplacement post-dates this deformational phase. The tectonic transposition of the D1 phase by the second phase of deformation does not allow to precise its orientation. At map scale (Figure 2), the metadiorite shows an elongated shape parallel to the orientation of the L2 lineation and to the S2 schistosity strike; this points to the syn-D2 emplacement of the magmatic body. Furthermore, the intense solid state deformation of the metadiorite and the fact that it shows the same structural characteristics as the gneiss, with respect to the D2 phase implies that the metadiorite was emplaced during the D2 deformational phase. Following D2, the metadiorite and the host gneisses experienced the same structural evolution; the distribution of S2 poles in the stereonet display, both in the metadiorite and the gneisses, regional folds with NE-SW trending axes (Figure 2). The orientation of D1 is difficult to determine; it could correspond to the N-S kinematic direction during the early Panafrican tectonic evolution which includes thrusting and shortening leading to crustal thickening (Ngako et al., 2008). The regional main strain direction during the D2 deformational phase was NE-SW as revealed by the orientation of the L2 stretching lineation. As the D3 is concerned, the major stress is orientated NW-SE, perpendicular to the regional F3 axial plane.

RESULTS

Geochemistry and $^{207}Pb/^{206}Pb$ geochronology

Chemical data of representative metadiorite samples are presented in Table 1. SiO_2 contents range from 46 to 66 wt%. In the SiO_2 versus ($Na_2O + K_2O$) diagram (Figure 3a), the samples were scattered but are mainly plotted in the fields of diorite and quartz diorite. The Na_2O/K_2O ratio varies between 1.35 and 2.55 with the exception of samples Me1b and Me1c which show ratios of 0.20 and 0.45, respectively. The metadiorite samples define a medium- to high-K calc-alkaline suite (again with the exception of samples Meb1 and Me1c with plots in the shoshonitic field in Figure 3b). ASI (A/CNK = [Al_2O_3/(CaO+Na_2O+K_2O) mol %]) (Table 1) varies from 0.6 to 0.9, pointing to an I-type character (White and Chappell, 1977).

The studied samples showed a wide variation of trace element contents (Ni: 17-70 ppm; Cr: 66-178 ppm; Y: 22-62 ppm; Pb: 8.8-24 ppm; Rb: 40-108 ppm; Sr: 188-630 ppm; Ba: 935-1424 ppm). The K/Rb ratio is 775 for Me1b and between 201 and 374 for the other samples, and the Rb/Sr ratio was less than 0.6. Normalized trace element and REE patterns are shown in Figure 4. The samples displayed negative anomalies in Nb, Ta, and Ti and a positive anomaly in K (Figure 4a). They exhibited moderate enrichment in LREE with respect to HREE (Figure 4b): $(La/Yb)_N$ = 9.5 – 11.3, $(La/Sm)_N$ = 2.8-3.0, $(Gd/Yb)_N$ = 1.9-2.1 and had moderate negative Eu anomalies (Eu/Eu* =0.80-0.83) and similar total REE concentrations (∑REE = 174-195 ppm).

Photographs and CL images of representative zircon grains of the metadiorite are shown in Figure 5a. The zircons are euhedral to subhedral in shape with euhedral oscillatory zonation and high-luminescence rims in some grains. They showed no obvious core domains and revealed many inclusions, probably of Th-rich minerals such as thorite ($ThSiO_4$) or thorianite [$(Th,U)O_2$]. The results of Pb evaporation of representative zircon grains are shown in Tables 2a and 2b. U/Th ratios varied from one grain to another and from one heating step to another. With the exception of two grains (3 and 6 of sample Me), the U/Th ratios generally increased with increasing heating temperature. In contrast, sample ZGo1 showed a decrease of the U/Th ratio in the higher heating steps. The $^{204}Pb/^{206}Pb$ ratios were generally <0.001. The $^{207}Pb/^{206}Pb$ ages ranged from 601.3 ± 0.8 Ma to 628.9 ± 4.7 Ma. In sample ZGo1, the $^{207}Pb/^{206}Pb$ ages ranged from 582.1 ± 7.8 Ma to 633.2 ± 3.9 Ma. There is a good reproducibility of the $^{207}Pb/^{206}Pb$ ages of the different heating steps, which allowed the determination of weighted mean ages of 614.1 ± 3.9 Ma (sample Me) and 619.8 ± 9.8 Ma (sample ZGo1) (Figure 5b, 5c; Table 2a, 2b).

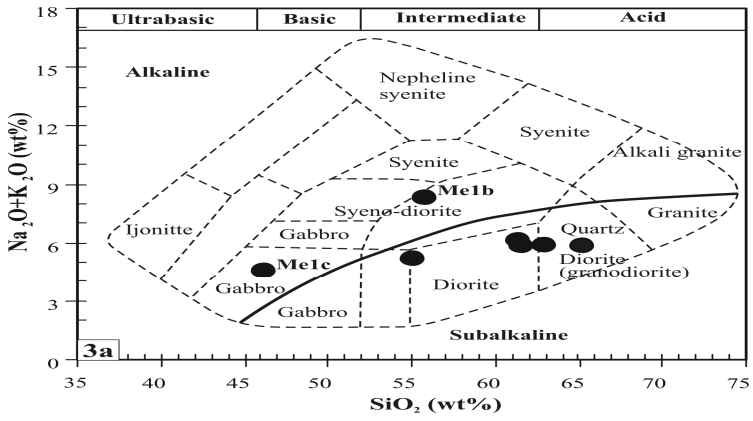

Figure 3a: Classification of the studied samples in the SiO_2 vs K_2O diagram (Wilson, 1989).

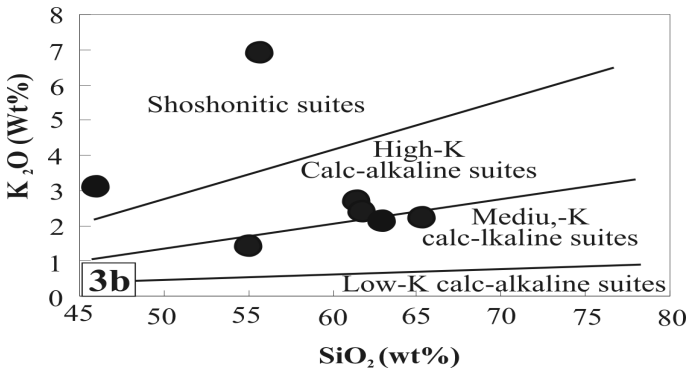

Figure 3b: Distribution of the Méiganga metadiorite samples in the K_2O versus SiO_2 diagram with compositional domains of the different calc-alkaline series, after Rickwood (1989).

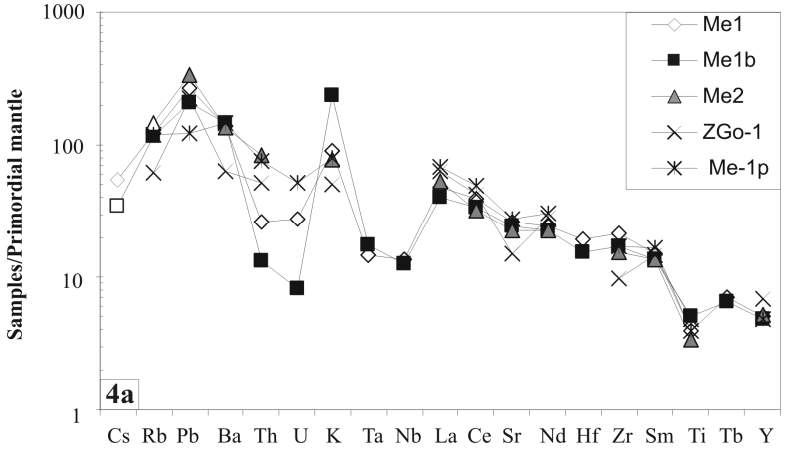

Figure 4a: Primordial normalised trace elements pattern for the metadiorite of Méiganga.
Normalisation values are from Mc Donough et al. (1992).

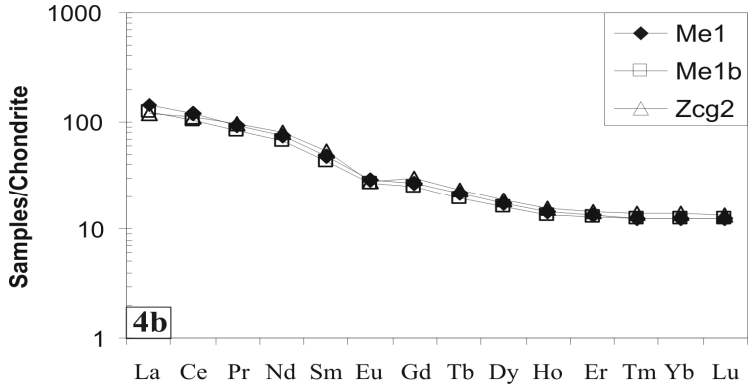

Figure 4b: Chondrite-normalised REE pattern for the Méiganga metadiorite.
Normalisation values are from Mc Donough and Sun (1995).

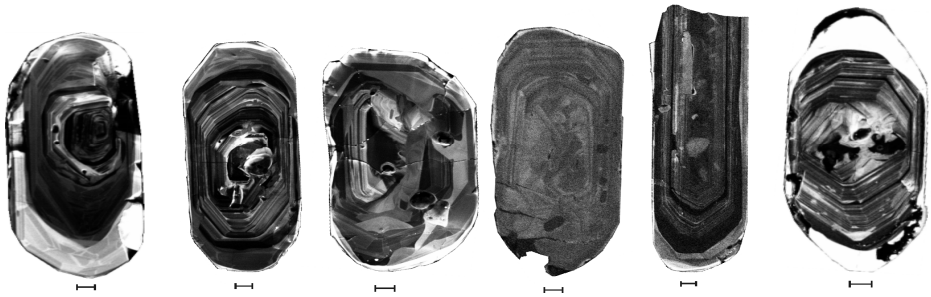

Figure 5a: Cathodoluminescence images of representative zircon crystals of the metadiorite (sample Me). Scale bar corresponds to 20µm.

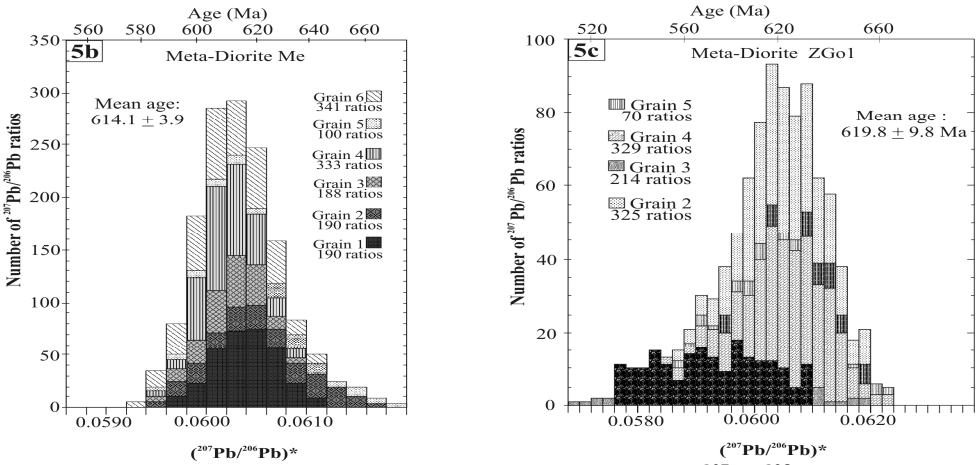

Figure 5b and 5c: Histograms showing the distribution of radiogenic $^{207}Pb/^{206}Pb$ ratios obtained from evaporation analyses of zircons grains (5b: sample Me, 5c: sample ZGo1).

Table 1: Geochemical composition of the Méiganga metadiorite.

Rock type	**Metadiorite**						
Samples	**Me1**	**Me1b**	**Me2**	**ZGo-1**	**Me-1p**	**Me1c**	**Yob1**
SiO_2	61.442	55.659	65.247	55.01	61.72	46.113	62.934
TiO_2	0.846	1.066	0.722	1.04	0.83	1.852	0.61
Al_2O_3	16.23	13.44	15.38	16.36	16.41	12.47	14.23
Fe_2O_3	6.688	7.978	5.366	9.20	6.00	16.443	6.671
MnO	0.121	0.122	0.103	0.16	0.11	0.285	0.115
MgO	3.31	4.41	2.60	4.18	3.10	7.91	2.49
CaO	5.40	6.35	4.48	7.75	5.18	7.85	6.21
Na_2O	3.54	1.40	3.57	3.69	3.57	1.40	3.78
K_2O	2.60	6.92	2.27	1.45	2.33	3.13	2.10
P_2O_5	0.25	2.09	0.192	0.23	0.24	0.537	0.688
LOI	0.51	0.73	0.41	0.42	0.70	0.86	0.43
Sum	101.16	101.21	100.56	99.66	100.42	99.12	100..65
Na_2O+K_2O	6.14	8.32	5.84	5.14	5.90	4.53	5.88
Na_2O/K_2O	1.36	0.20	1.57	2.54	1.54	0.45	1.80
A/CNK	0.9	0.6	0.9	0.8	0.9	0.6	0.7

Mg#	0.50	0.52	0.49	0.47	0.51	0.90	0.87
Ba	966	1012	936	447	1009	935	1424
Co	21.2	41.3	15.7	28.1	18.7	44.6	58.9
Cr	81.8	162.1	126.4	163.0	65.8	177.7	124.4
Ni	30.1	70.0	54.0	44.7	17.3	56.1	60.9
Rb	77.74	74.06	93.5	39.7	75.3	107.50	46.70
Sr	556	513	469	313	576	187	630
V	135.5	138.1	104.0	215.2	118.2	347.6	97.3
Y	22.9	21.8	23.6	30.9	22.0	61.8	29.1
Zn	90.1	94.7	64.1	110.3	73.9	208.7	73.2
Zr	237	189	172	108	189	265	323
K	21574	57426	18859	12044	19308	25965	17465
La	34.01	28.66	37.90	45.0	48.4	42.0	102.6
Ce	71.81	62.42	59.0	77.9	91.4	124.6	198.6
Pr	8.58	7.67					
Nd	33.38	30.47	30.6	38.2	42.1	72.1	71.5
Sm	6.60	6.03	6.0	6.5	7.3	10.6	11.3
Eu	1.61	1.53	1.4	1.4	1.8	1.6	2.2
Gd	5.26	4.91					
Tb	0.77	0.71					
Dy	4.27	4.01					
Ho	0.79	0.75					
Er	2.18	2.11					
Tm	0.31	0.31					
Yb	2.05	2.04	2	2.9	1.8	5.5	2.2
Lu	0.30	0.31					
Hf	6.03	4.81					
Ta	0.60	0.71					
W	7.36	185.3					
Pb	19.05	14.69	23.7	15.8	8.8	12.2	20.2
Th	2.22	1.11	7	4.3	6.3	0.9	15,8
U	0.57	0.17	b.d.l.*	b.d.l.	1.1	b.d.l.	1
Nb	9.75	8.93	b.d.l.	b.d.l.	b.d.l.	32.5	37.6
Be	2.22	2.07					
Cs	1.27	0.79					
Cu	14.32	44.96					
Ga	22.59	21.3					
Ge	1.5	1.41					
Mo	b.d.l.	1.19					
Sn	2.11	2.21					
∑REE	194.89	173.79					
K/Rb	277	775	202	303	256	241	374
Rb/Sr	0.14	0.14	0.20	0.13	0.13	0.57	0.07
Th/U	3.88	6.49			5.73		15.8
Sr/Y	24.23	23.50	19.89	10.14	26.19	3.03	21.64
La_N/Yb_N	11.28	9.54				5.19	31.68
Eu/Eu*	0.80	0.83					

* below detection limit

Table 2a: Zircon evaporation data including radiogenic $^{207}Pb/^{206}Pb$ ratios and corresponding ages for sample Me.

Sample and zircon n° (a,b = Temp. step	**Evap. temp °C**	**No of ratios**	**U/Th* ratio**	**$^{206}Pb/^{208}Pb$ ratio**	**$^{204}Pb/^{206}Pb$ ratio**	**$^{207}Pb/^{206}Pb$ ratio**	**$^{207}Pb/^{206}Pb$ age (Ma) 2σ error**
Me-1a	1400	187	1.11	3.58	0.000049	0.060406 ± 048	618.2 ± 1.6
Me-1b	1420	139	1.55	4.98	0.000029	0.060394 ± 053	617.8 ± 1.9
Me-2a	1420	140	2.32	8.25	0.000372	0.060594 ± 101	624.9 ± 3.6
Me-3a	1400	126	2.44	7.98	0.000072	0.059935 ± 023	601.3 ± 0.8
Me-3b	1420	188	1.88	6.10	0.000054	0.060223 ± 043	611.7 ± 1.6
Me-4a	1400	148	1.90	6.12	0.000042	0.060240 ± 040	612.2 ± 1.4
Me-4b	1420	185	1.92	6.60	0.000319	0.060193 ± 042	610.6 ± 1.5
Me-5a	1380	100	2.01	6.57	0.000076	0.060706 ± 654	628.9± 4.7
Me-6a	1380	118	1.82	5.91	0.000073	0.060155 ± 071	609.2 ± 2.6
Me-6b	1420	223	1.78	5.88	0.000156	0.060265 ± 054	613.1 ± 1.9
Mean 1a, 1b, 2a, 3b, 4a, 4b, 5a, 6a, 6b.		1554	*MSWD = 0.53;*	*Probability = 0.85*			*614.1 ± 3.9*

*calculated

Table 2b: Zircon evaporation data including radiogenic $^{207}Pb/^{206}Pb$ ratios and corresponding ages for sample ZGo1.

Sample and zircon number (a,b,c = Temp. step	**Evap. temp °C**	**No of ratios**	**U/Th* ratio**	**$^{206}Pb/^{208}Pb$ ratio**	**$^{204}Pb/^{206}Pb$ ratio**	**$^{207}Pb/^{206}Pb$ ratio**	**$^{207}Pb/^{206}Pb$ age (Ma) 2σ error**
ZGo1-2a	1380	105	1.57	5.13	0.000115	0.060297 ± 161	614.3 ± 5.8
ZGo1-2b	1400	112	1.53	4.92	0.000040	0.060519 ± 084	622.3 ± 3.0
Zgo1-2c	1420	108	1.45	4.69	0.000040	0.060643 ± 130	626.6 ± 4.6
ZGo1-3a	1410	114	1.59	5.20	0.000115	0.059406 ± 210	582.1 ± 7.8
ZGo1-3b	1430	100	1.42	4.61	0,000115	0.059465 ± 205	584.2 ± 7.6
ZGo1-4a	1400	112	1.55	5.17	0.000235	0.060429 ± 151	619.0 ± 5.4
ZGo1-4b	1420	109	1.45	4.69	0.000071	0.060828 ± 109	633.2 ± 3.9
ZGo1-4c	1440	107	1.50	4.87	0.000088	0.060477 ± 133	620.7 ± 4.8
ZGo1-5a	1400	70	1.16	3.75	0.000073	0.060657 ± 226	627.1 ± 8.1
Mean 2a, 2b, 2c, 3a, 3b, 4a, 4b, 4c, 5a		937		MSWD = 0.87; Probability = 0.54			619.8 ± 9.8

*calculated

DISCUSSION

Implications from geochemistry

The studied samples displayed chemical characteristics of medium-K calc-alkaline to shoshonitic granitoids and possessed I-type features as defined by Chappell and White (1974) and Chappell and Stephens (1988). They have a very weak anomaly negative Eu due to minor fractionation of plagioclase or to the fact that the parental magma of the diorite was in equilibrium with a plagioclase-bearing mantle source. The heavy-REE concentration of 10 to 20 times chondritic shows that garnet was absent from the original source. The negative anomalies in Nb, Ta, Ti and positive anomaly in K reflect geochemical source characteristics of the metadiorite protolith and provide evidence for the contribution of continental crustal material to the magma source (Taylor and McLennan, 1985; Barbarin, 1999). Negative Nb-Ta-Ti anomalies attest a subduction zone environment in which this crust was formed originally but these geochemical features are often retained during crustal reprocessing and can also be found in collisional-type granitoids (Pearce et al., 1984).

The syn-D2 emplacement and the $^{207}Pb/^{206}Pb$ ages indicate that this pluton dates the D2 deformation phase. The D2 event is thus interpreted to have occurred between 619 ± 9.8 Ma and 614 ± 3.9 Ma in the Méiganga region.

Regional timing of the D2 deformation event

D2 deformation and coeval magmatism in the Panafrican fold belt in Cameroon was dated at 600-580 Ma by Toteu et al. (1987, 2001). The Méiganga metadiorite gives similar older ages within the error limit to the ages obtained for granites from eastern Cameroon (614 ± 41 Ma and 621 ± 15 Ma, Rb-Sr whole-rock isochron: Soba et al., 1991). A similar age of 615 ± 27 Ma (U-Th-Pb monazite) has been obtained for a biotite muscovite granite in the north of Ngaoundéré which was syn- to late-tectonically emplaced relative to D2 (Tchameni et al., 2006). Syntectonic D2 granitoids in Tibati area, 300 km west of Méiganga, yield a U–Pb zircon age of 620 ± 30 Ma (Nzenti et al., 2006). Syn-D2 granitoids of western Cameroon were dated at 609-557 Ma (Kwékam et al., 2010; Nguiessi-Tchankam et al., 1994, 1997; Talla, 1995; Tagne-Kamga, 2003). This age is close to that of the syn-D3 granites dated at 601-558 Ma in the Méiganga area (Ganwa, 2005). All these rocks are characterized by discrete magmatic foliation and weak solid-state deformation, as opposed to the Méiganga metadiorite which shows the same penetrative solid-state deformation as the host gneisses. Nevertheless, we cannot completely rule out that granitoids of different age were generated in response to the same regional tectonomagmatic process. The D2 event could have started earlier in the Méiganga and Tibati areas and might have progressed south-westward to the western Cameroon area. Such scenario would be in line with the collision model of Ngako et al. (2008) in which the Saharan rigid prong penetrated into the São Francisco–Congo Craton between 640 and 580 Ma and generated intense deformation in northwestern Cameroon. In this case, the D2 deformational phase was diachronic in the Adamawa-Yade Domain of the CAFB. Diachronism in the tectonomagmatic event has been also demonstrated in the Macururé Domain of the Sergipano Belt (Bueno et al., 2009) in the Borborema Province (NE Brazil). Such similarities suggest that NE Brazil and Central Africa underwent the same tectonomagmatic history during the Neoproterozoic era.

ACKNOWLEDGEMENTS

The German Academic Exchange Service (DAAD) is highly acknowledged for supporting the research stay of the first author (GAA) at the University of Tübingen (Germany). The anonymous reviewers are thanked for their constructive remarks.

REFERENCES

Altherr R, Holl A, Hegner E, Langer C, Kreuzer H. 2000. High-potassium, calc-alkaline I-type plutonism in the European Variscides: northern Vosges (France) and northern Schwarzwald (Germany). *Lithos*, **50**: 51–73.

Barbarin B. 1999. A review of the relationships between granitoid types, their origins and geodynamic environments. *Lithos*, **46**: 605–626.

Bueno JF, Oliveria EP, McNaughton NJ, Laux JH. 2009. U-Pb dating of granites in the Neoproterozoic Sergipano Belt, NE-Brazil: Implications for the timing and duration of continental collision and extrusion tectonics in the Borborema province. *Gondwana Research*, **15**: 86–97.

Chappell BW, Stephens WE. 1988. Origin of infracrustal (I-type) granite magmas. *Transactions of the Royal Society of Edinburgh: Earth Sciences*, **79**: 71–86.

Chappell BW, White AJR. 1974. Two contrasting granite types. *Pacific Geology*, **8**: 173–174.

Chen F, Siebel W, Satir M. 2002. Zircon U–Pb and Pb-isotope fractionation during stepwise HF-acid leaching and chronological implications. *Chemical Geology*, **191**: 155–164.

Cocherie A, Guerrot C, Rossi P. 1992. Single-zircon dating by stepwise Pb evaporation: Comparison with other geochronological techniques applied to the Hercynian granites of Corsica, France. *Chemical Geology*, **101**: 131–141.

Djouka-Fonkwé ML, Schulz B, Schüssler U, Tchouankoué J-P, Nzolang C. 2007. Geochemistry of the Bafoussam Pan-African I- and S-type granitoids in western Cameroon, *Journal of African Earth Sciences*, **50**: 148-167.

Ganwa AA. 2005. Les granitoïdes de Méiganga: étude pétrographique, géochimique, structurale et géochronologique. Leur place dans la chaîne panafricaine. Thèse de Doctorat d'État, Université de Yaoundé I, 162 pp.

Kober B. 1986. Whole grain evaporation for 207Pb/206Pb-age investigations on single zircons using a double-filament thermal ion source. *Contribution to Mineralogy and Petrology*, **93**: 482–490.

Kober B. 1987. Single zircon evaporation combined with Pb + emitter bedding for 207Pb/206Pb-age investigations using thermal ion mass spectrometry, and implications in zirconology. *Contribution to Mineralogy and Petrology*, **96**: 63–71.

Kröner A, Willner AP. 1998. Time of formation and peak of Variscan HP–HT metamorphism of quartz-feldspar rocks in the central Erzgebirge, Saxony, Germany. *Contribution to Mineralogy and Petrology*, **132**: 1–20.

Kwékam M, Liégeois J-P, Njonfang E, l Affaton P, Hartmann G, Tchoua F. 2010. Nature, origin and significance of the Fomopéa Pan-African high-K calc-alkaline plutonic complex in the Central African fold belt (Cameroon). *Journal of African Earth Sciences*, **57**: 79–95

Lasserre M. 1961. Etude géologique de la partie orientale de l'Adamaoua (Cameroun Central) et les principales sources minéralisées de l'Adamaoua. *Bulletin de la Direction des Mines et Géologie du Cameroun*, **4**: 131.

Mc Donough WF, Sun SS. 1995. The composition of the Earth. *Chemical Geology*, **120**: 223–253.

McDonough WF, Sun SS, Ringwood AE, Jagoutz E, Hofmann AW. 1992. Potassium, rubidium and cesium in the Earth and Moon and the evolution of the mantle of the Earth. *Geochimica et Cosmochimica Acta*, **56**: 1001-1012.

Ngako V, Affaton P, Njonfang E. 2008. Pan-African tectonics in northwestern Cameroon: Implication for the history of western Gondwana. *Gondwana Research*, **14**: 509–522.

Nguiessi-Tchankam C, Nzenti J-P, Nsifa EN, Tempier P, Tchoua FM. 1997. Les granitoïdes calco-alcalins, syncisaillement de Bandja dans la chaîne panafricaine nord équatoriale au Cameroun. *Comptes Rendus de l´Académie Sciences,* **325**: 95–101.

Nguiessi-Tchankam C, Vialette Y. 1994. Données géochronologiques (Rb–Sr, Pb–Pb, U–Pb) sur le complexe plutonique de Bandja (Centre–Ouest Cameroun). *Comptes Rendus de l´Académie Sciences,* **319**: 317–324.

Njanko T, Nédélec A, Affaton P. 2006. Syn-kinematic high-K calc-alkaline plutons associated with the Pan-African Central Cameroon shear zone (W-Tibati area): Petrology and geodynamic significance. *Journal African Earth Sciences,* **44**: 494–510.

Njanko T, Nédélec A, Kwékam M, Siqueira R, Esteban L. 2010. Emplacement and deformation of the Fomope´a pluton: Implication for the Pan-African history of Western Cameroon. *Journal of Structural Geology*, xxx : 1–15.

Nzenti JP. 1994. L'Adamaoua panafricain (région de Banyo) une zone clé pour un modèle géodynamique de la chaîne panafricaine nord équatoriale au Cameroun. Thèse Doctorat d'Etat Univ. Cheick Anta Diop-Univ de Nancy I, 176 pp.

Nzenti JP, Badibanga Kapajika, Worner G, Lubala Toto R. 2006. Syn-kinematic emplacement of granitoids in a Pan-African shear zone in Central Cameroon. *Journal African Earth Sciences,* **45**: 74–86.

Nzolang C, Kagami H, Nzenti JP, Holtz F. 2003. Geochemistry and preliminary Sr–Nd isotopic data on the Neoproterozoic granitoids from the Bantoum area, west Cameroon: evidence for a derivation from a Paleoproterozoic Archean crust. *Polar Geoscience,* **16**: 196–226.

Pearce JA, Harris NBW, Tindle AG. 1984. Trace element discrimination diagrams for the tectonic interpretation of granitic rocks. *Journal of Petrology,* **25**: 956–983.

Penaye J, Toteu SF, Michard A, Bertrand JM, Dautel D. 1989. Reliques granulitiques d'âge protérozoïque inférieur dans la zone mobile panafricaine d'Afrique centrale au Cameroun : géochronologie U-Pb sur zircons. *Comptes Remndus Académie Sciences,* **309**: 315-318.

Rickwood PC. 1989. Boundary lines within petrologic diagrams which use oxides of major and minor elements. *Lithos,* **22**: 247–264.

Siebel W, Blaha U, Chen F, Rohrmüller J. 2005. Geochronology and geochemistry of a dyke–host rock association and implications for the formation of the Bavarian Pfahl shear zone, Bohemian Massif. *International Journal of Earth Sciences,* **94**: 8–23.

Soba D, Michard A, Toteu SF, Norman DI, Penaye J, Ngako V, Nzenti J-P, Dautel D. 1991. Données géochronologiques nouvelles (Rb–Sr, U–Pb, Sm–Nd) sur la zone mobile panafricaine de l´Est Cameroun: âge Protérozoïque supérieur de la série de Lom. *Comptes rendus de l'Académie des Sciences* **315**: 1453–1458.

Tagne-Kamga G. 2003. Petrogenesis of the Neoproterozoic Ngondo Plutonic complex (Cameroon, west central Africa): a case of late-collisional ferro-potassic magmatism. *Journal of African Earth Sciences,* **36**: 149–171.

Tagne-Kamga G, Mercier E, Rossy M, Nsifa NE. 1999. Syn-kinematic emplacement of the Pan-African Ngondo igneous complex (west Cameroon, central Africa). *Journal of African Earth Sciences,* **28**: 675–691.

Talla V. 1995. Le Massif granitic panafricain de Batié (Ouest - Cameroun): Pétrologie

-Pétrostructurale - Géochimie. Ph.D Thesis, University of Yaoundé I, 144 pp.

Taylor, RS, McLennan SM. 1985. *The Continental Crust: its Composition and Evolution*. Blackwell: Oxford; 312.

Tchameni R, Pouclet A, Penaye J, Ganwa AA, Toteu SF. 2006. Petrography and geochemistry of the Ngaoundéré Pan-African granitoids in Central North Cameroon: Implications for their sources and geological setting. *Journal of African Earth Sciences*, **44**: 511–529.

Toteu SF, Michard A, Bertrand JM, Rocci G. 1987. U/Pb dating of Precambrian rocks from northern Cameroon, orogenic evolution and chronology of the Pan-african belt of Central Africa. *Precambrian Research*, **37**: 71-87.

Toteu SF, Van Schmus WR, Penaye J, Michard A. 2001. New U–Pb and Sm–Nd data from north-central Cameroon and its bearing on the pre-Pan African history of central Africa. *Precambrian Research*, **108**: 45–73.

Toteu SF, Penaye J, Poudjom Djomani Y. 2004. Geodynamic evolution of the pan-African belt in central Africa with special reference to Cameroon. *Canadian Journal of Earth Sciences*, **41**: 73–85.

Wiedenbeck M, Alle P, Corfu F, Griffin WL, Meier M, Oberli F, Von Quadt A, Roddick JC, Spiegel W. 1995. Three natural zircon standards for U–Th–Pb, Lu–Hf, trace element and REE analyses, *Geostandard Newsletters*, **19**: 1–23.

Wilson M. 1989. *Igneous Petrogenesis*. Unwin Hyman: London.